HHS Public Access

Author manuscript

Invest New Drugs. Author manuscript; available in PMC 2019 October 01.

Published in final edited form as:

Invest New Drugs. 2018 October ; 36(5): 743–754. doi:10.1007/s10637-017-0558-5.

Sphingadienes show therapeutic efficacy in neuroblastoma *in vitro* and *in vivo* by targeting the AKT signaling pathway

Piming Zhao[1], **Ana E. Aguilar**[1,2,3], **Joanna Y. Lee**[1,2], **Lucy A. Paul**[1], **Jung H. Suh**[1], **Latika Puri**[1,4], **Meng Zhang**[1], **Jennifer Beckstead**[1], **Andrzej Witkowski**[1], **Robert O. Ryan**[1], and **Julie D. Saba**[1,*]

[1]UCSF Benioff Children's Hospital Oakland, Children's Hospital Oakland Research Institute, 5700 Martin Luther King Jr. Way, Oakland, CA, 94609, USA

Abstract

Neuroblastoma is a childhood malignancy that accounts for approximately 15% of childhood cancer deaths. Only 20–35% of children with metastatic neuroblastoma survive with standard therapy. Identification of more effective therapies is essential to improving the outcome of children with high-stage disease. Sphingadienes (SD) are growth-inhibitory sphingolipids found in natural sources including soy. They exhibit chemopreventive activity in mouse models of colon cancer, where they mediate cytotoxicity by inhibiting key pro-carcinogenic signaling pathways. In this study, the effect of SD on neuroblastoma was analyzed. Low micromolar concentrations of SD were cytotoxic to transformed and primary neuroblastoma cells independently of N-Myc amplification status. SD induced both caspase-dependent apoptosis and autophagy in neuroblastoma cells. However, only inhibition of caspase-dependent apoptosis protected neuroblastoma cells from SD-mediated cytotoxicity. SD also inhibited AKT activation in neuroblastoma cells as shown by reduced phosphorylated AKT levels. Pre-treatment with insulin attenuated SD-mediated cytotoxicity *in vitro*. SD-loaded nanoparticles (NP) administered parenterally to immunodeficient mice carrying neuroblastoma xenografts resulted in cytotoxic levels of SD in the circulation and significantly reduced tumor growth compared to vehicle-treated controls. Analysis of tumor extracts demonstrated reduced AKT activation in tumors of mice

[*]To whom correspondence should be addressed. jsaba@chori.org; Phone 510-450-7690.
[2]These authors contributed equally to this work.
[3]Currently at Arnold Palmer Hospital for Children, 92 W Miller St MP 318 2nd floor, Orlando, FL 32806 USA
[4]Currently at St Jude Children's Research Hospital, 262 Danny Thomas Pl Memphis, TN 38105, USA

Compliance with Ethical Standards

Conflicts of Interest: Author Piming Zhao declares that he has no conflict of interest. Author Ana E. Aguilar declares that she has no conflict of interest. Author Joanna Y. Lee declares she has no conflict of interest. Author Lucy A. Paul declares she has no conflict of interest. Author Jung H. Suh declares he has no conflict of interest. Author Latika A. Puri declares that she has no conflict of interest. Author Meng Zhang declares he has no conflict of interest. Author Jennifer Beckstead declares she has no conflict of interest. Author Andrzej Witkowski declares he has no conflict of interest. Author Robert O. Ryan declares he has no conflict of interest. Author Julie. D Saba declares she has no conflict of interest.

Contributions: All authors contributed substantially to the study. Data were generated and analysed by PZ, AEA, LAP, JYL, JHS, LP, MZ, JB and AW. ROR contributed to the design of some of the studies and interpretation of results. JDS designed the overall study, interpreted all results and wrote the manuscript. All authors reviewed the manuscript for accuracy and contributed to the writing of the manuscript.

Ethical Approvals: Human tumor and nonmalignant tissues utilized in this study were acquired in accordance with an approved UCSF Benioff Children's Hospital Oakland Institutional Review Board protocol and with informed consent. All animal experiments conducted in this study were performed in accordance with an approved UCSF Benioff Children's Hospital Oakland Institutional Animal Care and Use Committee protocol.

treated with SD-NP compared to controls treated with empty NP. Our findings indicate SD are novel potential chemotherapeutic agents that promote neuroblastoma cell death and reduce tumorigenicity *in vivo*.

Keywords

sphingadienes; sphingolipids; neuroblastoma; PI3K; AKT; nanoparticle

Introduction

Neuroblastoma is a highly lethal malignancy of childhood. It is an embryonal malignancy of the sympathetic nervous system arising from neuroblasts (pluripotent sympathetic cells) and represents the most common extra cranial solid tumor in infancy [1–3]. More than 50% of afflicted children present with metastatic disease, and the current survival rate for patients presenting with high-stage disease is 20–35% [4, 5]. Neuroblastoma has a heterogeneous clinical presentation and course [6]. Tumors may regress spontaneously, mature into benign ganglioneuromas, or present as advanced/metastatic disease that carries a poor prognosis [4, 7]. Current therapies include surgery, chemotherapy, immunotherapy, bone marrow transplant and radiation [1, 5, 8, 9]. Research efforts to identify new and more effective therapies are essential to improve the outcome of affected children.

Sphingolipids are a complex family of lipids built upon a sphingoid base backbone. Higher order sphingolipids are primarily located in the plasma membrane, where they serve structural membrane functions. The composition of membrane sphingolipids changes dramatically during carcinogenesis [10]. Novel or aberrantly glycosylated sphingolipids that are enriched in tumor cell plasma membranes have been identified as tumor-specific antigens and are targeted therapeutically [11–14]. One of the most promising new approaches for the treatment of neuroblastoma involves passive immunotherapy targeting the neuroectodermal sphingolipid ganglioside GD2 [8, 15]. Anti-GD2 monoclonal antibodies may act by mediating antibody-dependent cellular cytotoxicity (ADCC) and complement-dependent cell cytotoxicity (CDC) [1, 4, 16, 17]. Membrane sphingolipids are regularly internalized and recycled [18], giving rise to bioactive intracellular metabolites involved in the regulation of cell proliferation, differentiation, migration and apoptotic and autophagic programmed cell death [10]. Thus, anti-GD2 and other sphingolipid-directed immunotherapies may exert cytotoxicity by mechanisms involving sphingolipid intermediates.

In contrast to the long history of targeting complex sphingolipids in neuroblastoma, the role of bioactive sphingolipid metabolites in the treatment of neuroblastoma has not been thoroughly explored. Sphingadienes (SD) are growth-inhibitory long chain sphingoid bases found in soybeans, insects, marine organisms and other natural sources [19]. SD contain an additional double bond compared to sphingosine, the most common mammalian sphingoid base sphingosine. This structural difference is thought to confer SD with their enhanced cytotoxicity [20]. SD induce colon cancer cell death and prevent intestinal tumorigenesis in murine models of colon cancer. We showed previously that SD inhibit PI3K/AKT-dependent

signaling by preventing AKT membrane translocation, thereby resulting in inhibition of protein translation and de-repression of apoptosis and autophagy [21]. SD have been shown to exert inhibitory effects on WNT signaling through a pathway involving PP2A, AKT and GSK3 beta [22]. Deregulation of the PI3K/AKT pathway has been shown to play a major role in cancer development and chemotherapy resistance [23]. AKT activation has been shown to be an indicator of poor prognosis in neuroblastoma [24].

In this study, we explored the potential of SD as therapeutic agents in neuroblastoma. Utilizing a combination of transformed and primary neuroblastoma lines, we show that SD are cytotoxic to neuroblastoma cells through a mechanism involving inhibition of AKT and induction of apoptotic cell death. A novel method of delivering SD parenterally using apolipoprotein (apo)-phospholipid nanoparticles (NP) was employed [25]. Administration of SD-NP to mice inhibited neuroblastoma xenograft growth and reduced AKT activation in tumor tissue extracts. These findings suggest that SD may be potentially useful as chemotherapeutic agents in neuroblastoma.

Materials and methods

Antibodies and reagents

SD are from Avanti Polar Lipids (Alabaster, AL). Antibodies against synaptophysin are from Millipore (Billerica, MA, USA). Antibodies against tyrosine hydroxylase (TH), phospho-AKT1/2/3 (Ser473), total AKT, LC3 and poly (ADP-ribose) polymerase (PARP) are from Cell Signaling Technology (Danvers, MA). Antibodies against GAPDH are from Santa Cruz Biotechnology (Santa Cruz, CA). Antibodies against β-actin and the compound 3-methyladenine (3-MA) are from Sigma-Aldrich (St. Louis, MO). Horseradish peroxidase-anti-rabbit IgG and FITC-anti-mouse IgG secondary antibodies are from Jackson Immuno Research Laboratories (West Grove, PA). DMEM:F12 with high glucose (DMEH-21), FBS, RPMI 1640, insulin and antibiotics are from UCSF Tissue Culture Facility (San Francisco, CA). Pan-caspase inhibitor Z-VAD-FMK is from Enzo Life Sciences (Farmingdale, NY). Bafilomycin A1 is from Cayman Chemical Company (Ann Arbor, MI).

Immunoblotting

Immunoblotting was performed as described [26]. Signals were visualized using the SuperSignal West-Pico kit (Fisher Scientific, Rockford, IL) and quantified by densitometry using ImageJ software (NIH).

Cell culture and transfections

Authenticated LAN-5 and KELLY neuroblastoma cell lines were purchased from UCSF Tissue Culture Facility (San Francisco, CA). Authenticated SHSY5Y cell line was purchased from ATCC (Rockville, MD, USA). LAN-5 and Kelly cells were grown in RPMI 1640 medium containing 10% FBS, 100 units/ml penicillin and 100 μg/ml streptomycin. SHSY5Y was grown in DMEM-H21 with 10% FBS, 100 units/ml penicillin and 100 μg/ml streptomycin. SD were dissolved in ethanol or DMSO. SD treatment was performed in serum free DMEH-H21 or RPMI1640 medium depending of the cell line and compared to the appropriate vehicle.

Establishment of primary cell lines from normal kidney tissue and neuroblastoma tumors

Primary human neuroblastoma cells were isolated from fresh tumor tissue from a stage IV N-Myc amplified adrenal mass. Primary human kidney cells were isolated from normal kidney tissue. Minced tissue was dissociated with papain (Worthington Biochemical Corporation, Lakewood, NJ) for 10–15 min at 37°C, triturated using a 5-ml pipette, and re-suspended in complete media (DMEM + 10% FBS). The suspension was filtered twice through 70 μm and 40 μm filters. The suspension was collected in a 15-ml tube and subjected to centrifugation at 1200 rpm for 10 min. The supernatant was aspirated and discarded, and cells were washed with PBS supplemented with Ca^{2+} and Mg^{2+} and subjected to centrifugation at 1000 rpm for 10 min. The supernatant was aspirated, and the cells were re-suspended in DMEM-high glucose with 10% FBS, 100 units/ml penicillin, 100 μg/ml streptomycin, 20 ng/ml EGF (Sigma-Aldrich, St. Louis, MO), 20 ng/ml recombinant human FGF (Preprotech, Rocky Hill, NJ), and fungizone 2.5 μg/ml (UCSF, San Francisco, CA), and seeded in a 10-cm dish for further propagation and characterization. Human tumor samples were obtained with informed consent in accordance with an approved Institutional Review Board Protocol.

Immunofluorescence

Cells were grown in a 4-well chamber slide until 70–80 % confluent. Cells were washed with cold PBS, fixed with 4% paraformaldehyde and permeabilized with 0.5% Triton-X 100. After blocking, cells were incubated in 5% goat serum and 0.1% Triton-X 100 in PBS for 1 h and then incubated overnight at 4°C with the primary antibody. Tyrosine hydroxylase and synaptophysin were tested. After washing, some cells were stained with DAPI and others with propidium iodide and mounted in Vectashield. Images were captures using a Zeiss Axioskop fluoresence microscope (Carl Zeiss, Thornwood, NY) and images were processed using Adobe Photoshop CS5.1 (Adobe, San Jose, CA).

Cell viability and cell death assays

Cells were analyzed for viability by [3-(4,5-dimethylthiazol-2-yl)-5-(3-carboxymethoxyphenyl)-2-(4-sulfophenyl)-2H-tetrazolium; MTS] assay using the CellTiter96® AqueousOne Non-Radioactive Cell Proliferation Assay (Promega, Madison, WI), which relies on formation of the formazan product of MTS by viable cells. After addition of the MTS to the media, cells were incubated at 37°C for 45–60 min, and the absorbance at 490 nm was measured. PARP cleavage and LC3 modification were measured by immunoblotting as described [21, 27] using 10% and 15% SDS-PAGE gels, respectively.

SD-NP preparation and characterization

Ten mg 1,2-dimyristoyl-sn-glycero-3-phosphocholine (DMPC; Avanti Polar Lipids) was dissolved in chloroform / methanol (3:1 v/v) and dried under a stream of N_2 gas, forming a thin film on the vessel wall. Residual organic solvent was removed under vacuum. The prepared lipids were then dispersed in 1 ml phosphate buffered saline (PBS; 20 mM sodium phosphate, 150 mM sodium chloride, pH 7.0) and 1.0 mg SD (from a stock solution in dimethylsulfoxide; DMSO) was added. Following this, 4 mg isolated recombinant apoA-I [28] was added and the solution (2 ml final volume) subjected to bath sonication, with the

sample temperature maintained between 22°C and 25°C. After sonication the turbid mixture became clear, indicating apolipoprotein/phospholipid complexes (e.g. NP) had formed. This solution was dialyzed overnight against PBS, pH 7.4, to remove DMSO using a 23 mm Spectra/Por dialysis membrane (Spectrum Labs) with a tubing molecular weight cutoff of 6–8 kDa filtered through a 0.22-μm sterile filter and stored at 4°C until use. Efficiency of SD incorporation into NP was determined to be 63.5% by quantifying SD in the pre- and post-dialysis solutions. Empty NP were prepared as described for SD-NP except that SD was omitted. Size exclusion chromatography was performed as described [29]. Two hundred μl of the sample were applied on a Perkin-Elmer Series 200 System equipped with 9.4 × 250 mm Zorbax GF-250 column equilibrated in 50 mM sodium phosphate plus 0.5 M sodium chloride buffer, pH 7.3, eluted with the same buffer at a flow rate of 1 ml/min, absorbance at 280 nm was recorded and 0.5 ml fractions were collected. SD was quantified as described below on a portion of selected fractions.

SD quantitation

To quantify SD amount incorporated into NP preparations, present in gel filtration fractions, and plasma levels, a novel LC/MS method we recently reported was utilized [30]. An Agilent 1290 UPLC system coupled with Agilent 6490 Triple Quadrupole (QqQ) mass spectrometer were used for analysis. Briefly, C17-sphingosine (d18:1/17:0, Avanti Polar lipids; 10 nmol) was added to samples prior to extraction as a quantitative internal standard. SD and C17-sphingosine were eluted on Zorbax SB-C18 column (Agilent) by isocratic delivery of mobile phase [LC-MS grade methanol containing 1 mM ammonium formate and 0.2% formic acid] at a flow rate of 1.0 ml/min. Analysis was carried out using multiple-reaction-monitoring (MRM) mode. The MRM transitions used for SD and C17-sphingosine detection were 298.2 →280.2 [collision energy (CE):8V]and 286.5→268.3 (CE 4,V), respectively. The general source settings in the positive ionization modes were as follows: gas temperature 200 °C; gas flow, 14 L min-1; nebulizer 20 psi; sheath gas temperature 250 °C; sheath gas flow 11 L min-1; capillary voltage 3000 V; and nozzle voltage; 0V. The fragmentor voltage of 380V and a dwell time of 15 ms were used for all mass transitions, and both Q1 and Q3 resolutions were set to nominal mass unit resolution.

Animals

To assess the impact of SD-NP i.p. delivery on plasma SD levels, a single dose of 5 mg/kg SD-NP was administered to 15 mice, followed by euthanasia of 3 mice per time point at 5 min, 10 min, 30 min, 2h and 8h after injection, with 3 additional mice euthanized at time 0 as controls. SD levels were measured in plasma as described in Methods. To assess the potential toxicity of SD-NP, mice were treated with SD-NP at 5 mg/kg/dose twice a day (10 mg/kg/d) or vehicle for five doses (n=3 per group), followed by euthanasia five days after the last dose. Blood was obtained by cardiac puncture and collected into EDTA-containing blood tubes for hematology tests or serum collection tubes for liver functions and blood chemistries. All blood tests were performed at the University of California at Davis Comparative Pathology Laboratory, and results were reported along with laboratory standard results for adult wild type Balb/c mice. For xenograft studies we chose to deliver SD-NP *in vivo* using a 5 mg/kg/dose twice a day (10 mg/kg/d) regimen. For xenograft studies, 6-week-old NOD-CB17-Prkdcscid immunocompromised female mice (Sz/J) (Jackson Labs Stock

No: 001303) were injected subcutaneously in both flanks with Kelly neuroblastoma cells. Briefly, 2×10^6 cells were suspended in PBS, mixed in a 1:1 ratio with Matrigel (BD Biosciences, USA) and injected subcutaneously into the mouse flank. Tumor size was measured using a digital caliper. Tumor volume was measured as described [31]. Mice were randomly allocated to each treatment group, and treatments were started once tumors reached 100 mm^3. Mice received either SD-NP (10 mg/kg/day) or vehicle in 250 μL twice daily by i.p. injection. Mice were euthanized at the humane endpoint, i.e., when tumors reached > 9% of the body weight based on the formula: Length $(cm)^2$ x Width (cm)/2 = volume. To measure the impact of SD on AKT activation in tumor tissues, tumor-bearing mice were injected with a single dose of either SD-NP or empty NP vehicle, followed by euthanasia 8 h after treatment. Euthanasia was performed by CO_2 inhalation. Tumors were harvested and flash-frozen in liquid nitrogen for molecular analysis as described above for immunoblotting. These studies were performed in accordance with an approved CHORI Institutional Animal Care and Use Committee protocol.

Statistical analysis

Statistical analysis on *in vitro* experimental data for sets of 3 or more data points was performed using Student's *t*-test. Statistical analysis on tumor growth was performed using two-way ANOVA followed by Tukey's post-test. P values< 0.05 were considered significant.

Results

SD inhibit the growth of transformed and primary neuroblastoma cells

To explore the potential of SD to serve as chemotherapeutic agents in neuroblastoma, we tested the impact of SD on the viability of Kelly neuroblastoma cells, which represent a transformed and N-Myc amplified neuroblastoma cell line. SD induced a dose- and time-dependent inhibition of viability in neuroblastoma cells as determined by MTS assay (Figure 1A–B). As low as 0.5 μM SD significantly compromised Kelly cell viability. Similar to the observed effects on Kelly cells, inhibition of viability was observed in two additional well-characterized neuroblastoma cell lines derived from patients with Stage IV disease, namely non-N-Myc amplified SHSY5Y cells and N-Myc-amplified LAN-5 cells after treatment with micromolar doses of SD (Supplementary Figure 1 A–C). In contrast to the effects on neuroblastoma cells, SD did not influence the viability of two non-malignant cell lines, NIH 3T3 fibroblasts and a primary cell line we derived from human embryonic kidney tissue (Figure 1C). To ascertain the impact of SD in a more physiological cell model of neuroblastoma, we derived a primary cell line from an abdominal neuroblastoma tumor surgically removed from a chemotherapy-naïve patient as described in Methods. To verify the authenticity of the primary cells, we performed immunofluorescence labeling to detect the neuronal markers tyrosine hydroxylase and synaptophysin, followed by immunofluorescence microscopy. Kelly neuroblastoma cells were used as a positive control. As shown in Supplementary Figure 2A, primary neuroblastoma cells were positive for both neuronal markers. Primary neuroblastoma cells behaved similar to transformed neuroblastoma cell lines, exhibiting reduced viability after treatment with low micromolar doses of SD (Supplementary Figure 2B).

SD induce neuroblastoma cell death by inducing apoptosis

The effect of SD detected in viability assays could be explained by an induction of cell death or cell cycle arrest. To distinguish between these two possibilities, we measured the percentage of cells undergoing cell death by the trypan blue assay. Trypan blue staining of LAN-5, Kelly and SHSY5Y cells treated with a range of SD concentrations confirmed that nearly 100% of neuroblastoma cells were nonviable after 48h of incubation with 10 μM SD (data not shown). To determine whether SD induced cell death by activating apoptosis, we measured the cleavage of the caspase-3 substrate PARP by immunoblotting whole cell extracts of Kelly cell cultures incubated with a range of SD concentrations for 6 h. As shown in the immunoblot in Figure 2A and image quantification graph in Figure 2B, PARP was intact in vehicle-treated cells, whereas the cleaved product was detectable in the extracts of cells treated with 5 and 10 μM SD. Similar results were observed in SHSY5Y and LAN-5 cells (data not shown). We have shown previously that SD can elicit cell death by inducing apoptosis and also by inducing autophagy [21]. To assess whether SD elicit autophagy in neuroblastoma cells, we measured the presence of unmodified and modified forms of the autophagy marker LC3. Autophagy was induced in cells treated with 5–10 μM SD, as shown by the presence of the processed form of LC3 (LC3II) (Figure 2C and D). Autophagy can serve as both a cell survival mechanism as well as a cell death pathway. To ascertain which of the two forms of programmed cell death elicited by SD in neuroblastoma cells was primarily responsible for causing their cell death, we pretreated Kelly cells with the autophagy inhibitors 3-MA or bafilomycin, or with the pan-caspase inhibitor of apoptosis, Z-VAD-FMK, followed by treatment with either vehicle or 10 μM SD. As shown in Figure 2E none of the autophagy inhibitors negatively impacted cell viability, as determined by MTS assay. In addition, pretreatment with 3-MA or bafilomycin did not protect the cells against SD-mediated cytotoxicity. In contrast, pretreatment with Z-VAD-FMK completely abrogated cell death in response to SD. These findings demonstrate that SD induce neuroblastoma cell death via apoptosis and not via autophagy.

SD mediate cytotoxicity in neuroblastoma cells by targeting AKT signaling

The ability of SD to induce both apoptosis and autophagy in neuroblastoma cells was reminiscent of the effects of SD in colon cancer cells. In the latter, SD have been demonstrated to mediate cytotoxicity by inhibiting the membrane translocation and activation of AKT, thereby preventing AKT signaling events that suppress both of these forms of programmed cell death [21, 22]. To measure the impact of SD on AKT signaling in neuroblastoma cells, Kelly cells were treated with 10 μM SD, followed by incubation for 1–6 h. Cells were harvested, and immunoblotting was performed on whole cell extracts to measure the abundance of Ser473-phosphorylated AKT, which corresponds to an activated form of AKT. As shown in Figure 3A and Supplemental Figure 3A, SD caused an inhibition of AKT detectible within 2 h after treatment, as shown by a reduction of phosphorylated AKT (P-AKT) relative to total AKT (T-AKT) in whole cell extracts. Apoptosis, indicated by the presence of PARP cleavage, was detectible at 4 h after treatment (Figure 3A and Supplemental Figure 3B). Treatment of Kelly cells with as low as 3 μM SD for 8 h reduced AKT activity and induced apoptosis indicated by PARP cleavage, as shown in Figure 3B and Supplemental Figures 3C–D. Similar results were observed in other neuroblastoma cell lines (data not shown). To test the role of AKT inhibition in mediating the cytotoxic effects of SD

on neuroblastoma cells, Kelly cells were pretreated for 1 h with insulin to activate the AKT signaling pathway, whereas other cells received vehicle pretreatment. Cells were then exposed to different amounts of SD up to 15 μM for 6h, followed by cell harvest and immunoblotting to detect PARP cleavage. As shown in Fig 3C and Supplemental Figure 3E, insulin pre-treated cells were protected from SD-mediated apoptosis. Consistent with this finding, Kelly cells pretreated with insulin for 6 h followed by treatment with 10 μM SD were resistant to SD-mediated cytotoxicity as shown by a significant increase in viability (Figure 3D).

Characterization of SD-loaded nanoparticles and plasma levels after intraperitoneal delivery

Based on our *in vitro* findings suggesting that SD are cytotoxic to neuroblastoma cells, it became important to ascertain the impact of SD on neuroblastoma tumorigenicity *in vivo*. SD are hydrophobic molecules that are insoluble in aqueous solution and challenging to deliver by a parenteral route. We have also found that orally delivered SD are only transiently detectible in the blood, which suggests they are rapidly metabolized [30]. Nanoparticles [NP] are nanoscale phospholipid particles that are stabilized by apolipoproteins and can serve as carriers for hydrophobic drugs [32]. Our previous experience with solubilization of the poorly absorbed compound curcumin using disk-shaped NPs and reduced toxicity of the antibiotic amphotericin B when delivered *in vivo* using NP suggested that they might be an effective delivery system for SD [25, 33–35]. To explore the utility of NP as a vehicle for solubilization and transport of SD, we generated apoA1-containing NP incorporating SD as described in Methods. Addition of apoA-I to an aqueous dispersion of DMPC/SD induced clarification of the reaction mixture with complete solubilization of the drug in a transparent solution. From these results, it is evident that apoA-I interacted with the lipid/drug mixture to form soluble, SD-bearing lipid complexes, similar to drug-bearing NP we described previously [25, 35]. Dialysis of the sample against PBS resulted in the loss of 36.5% of the original SD, as determined by quantification of SD in the pre- and post-dialysis mixture using LC/MS/MS, thus indicating an efficiency of loading of 63.5%. To further confirm that the SD was loaded on the NP, the sample was subjected to density gradient ultracentrifugation. After centrifugation, the tube contents were fractionated and analyzed for protein, SD and density. As shown in Figure 4A, the majority of the SD co-migrated with the apolipoprotein carrier in a heterogeneous population of higher molecular weight species as compared to empty NP. These results confirm that SD is contained within the NP. Like SD solutions in DMSO, SD-NP were cytotoxic to neuroblastoma cells in a dose-dependent fashion when delivered to neuroblastoma cell cultures (data not shown). We then examined plasma SD levels after treatment of wild type mice with SD-NP by intraperitoneal delivery. SD were undetectable at time 0, rose to approximately 2 μM at 10 min and peaked at 30 min at 4 μM. SD was detectable but less than 1 μM at 8h (Figure 4B). Thus, a cytotoxic plasma level of SD was achieved by delivery of SD-NP by parenteral delivery.

To assess potential toxicities of SD-NP administration, mice were treated with SD-NP at 5 mg/kg/dose or vehicle given i.p. for five consecutive doses (n=3/group). Blood chemistry, hematology and liver function tests were performed on mice five days after the last treatment

dose. As shown in Table 1, some values were significantly different between the two groups. For example, white blood cell count (WBC), red cell distribution width (RDW) and blood urea nitrogen (BUN) were significantly higher in SD-NP treated vs. control mice. Other values, including mean platelet volume (MPV), alkaline phosphatase and total protein (TP) were lower than controls. However, all blood chemistry, liver function and hematology test results for SD-NP treated and control mice fell within the normal limits for wild type mice as reported by the laboratory.

SD-NP inhibit growth and suppress AKT signaling in neuroblastoma xenograft tumors

We next treated NOD/SCID mice bearing Kelly neuroblastoma cell xenografts with SD-NP (n = 17) or control (n = 3). When the tumors reached 100 mm^3, mice received SD-NP at a dose of 10 mg/kg/d or vehicle by i.p. injection, and tumor growth was monitored daily with calipers. As shown in Figure 5A, average tumor size of SD-NP treated mice was significantly lower than that of control mice beginning on day 6 after starting the treatment and continuing through day 8. Whereas xenograft tumors grew appreciably from day 6 to day 8 in control mice, tumors in SD-NP treated mice did not grow significantly during the same time period. Representative tumors in mice injected with empty NP and SD-NP are shown in Figure 5B. We next sought to determine whether the reduction in tumor growth was accompanied by a change in AKT activation status within tumor tissue. Toward that end, an independent study was conducted in tumor-bearing mice that were treated with a single dose of either vehicle (n = 4) or SD-NP (n = 3) in 500 μL volume by i.p. injection, followed by euthanasia at 8 h after the treatment. The tumors were harvested and homogenized for molecular analysis. As shown in Figure 5C–D, immunoblotting of tumor extracts revealed a reduction in AKT activation (as determined by P-AKT/T-AKT) in the tumors of SD-NP treated mice compared to those of empty NP treated mice. These findings suggest that SD-NP inhibit tumor growth and reduce AKT activation in neuroblastoma xenografts *in vivo*.

Discussion

Here, we report the effects of a natural plant sphingolipid called SD in neuroblastoma. We have previously shown that SD exert cytotoxicity in colon cancer cells via inhibition of AKT and that short-term oral administration of SD prevents intestinal tumorigenesis without causing toxicity [22]. Our results show that SD are cytotoxic to neuroblastoma cells irrespective of N-Myc amplification status. The effects of SD were observed in primary and transformed neuroblastoma cell lines but not in primary or transformed nonmalignant cell lines. We found that SD induce apoptosis and autophagy when administered at low micromolar doses. However, the cytotoxicity of SD in neuroblastoma is mediated specifically by the induction of apoptosis.

Sphingolipid metabolism and bioactive metabolites have been implicated in neuroblastoma biology. Sphingosine kinase 2 (SphK2), one of two lipid kinases capable of converting sphingosine to the anti-apoptotic and pro-angiogenic sphingolipid sphingosine 1-phosphate (S1P), is overexpressed in neuroblastoma [36]. Villullas et al. reported expression of S1P receptors 2, 3, and 5 in neuroblastoma cells [37]. S1P influences the tumor

microenvironment in neuroblastoma by inducing VEGF expression via S1P2 [36]. Since VEGF is highly overexpressed in poor prognosis neuroblastoma, SphK2 overexpression and S1P generation could potentially promote neuroblastoma progression [36]. S1P also appaB, AKT/PI3K, and STAT3 [38]. Li et al. reported that FTY720, a sphingosine analogue and S1P receptor modulatory agent, exerts an antitumor effect on neuroblastoma cells by reducing SphK2 expression, thereby increasing sphingosine levels and inducing apoptosis in a caspase-independent manner [39]. Sphingosine and S1P have been reported to induce neuronal cell differentiation in neuroblastoma cells [38, 40]. Similar to sphingosine and S1P, ceramide induces neuronal cell differentiation via a mechanism mediated by PP2A [38]. Given that current neuroblastoma therapy aims at achieving tumor regression through cell differentiation, these findings may prove to be significant. Ceramide has been implicated in the regulation of programmed cell death [20, 41]. Czubowicz and colleagues report that ceramide induces cell death regulated through PARP/apoptosis-inducing factor (PARP/PAR/AIF) and S1P receptor signaling [42]. Kraveka et al. demonstrated that the *in vitro* target of fenretinide, a drug used for relapse and high-risk neuroblastoma, inhibits dihydroceramide desaturase, which is the enzyme that catalyzes the conversion of dihydroceramide to ceramide [43]. This suggests that dihydroceramide may be active against neuroblastoma and that DEGS1, the major active dihydroceramide desaturase in neuroblastoma cells, could function as a target in this disease. Combined with these cumulative observations, our findings regarding SD suggest that sphingolipid metabolites, intermediates, and/or synthetic analogs may have potential in neuroblastoma treatment.

SD caused a dose- and time-dependent inhibition of AKT activation in neuroblastoma cells, with effects in the low micromolar range. We observed similar results in other neuroblastoma cell lines. Importantly, pre-treatment with insulin protected neuroblastoma cells, inhibiting SD-mediated cytotoxicity and apoptosis. These findings suggest that in neuroblastoma, as in colon cancer cells, SD exert cytotoxic effects via suppression of AKT signaling. Deregulation of the PI3K/AKT pathway is a common event in human malignancies and plays a key role in cancer development, progression, and chemotherapy resistance. Tumors that show high levels of activated AKT have been shown to be more aggressive than those exhibiting low levels of AKT activation [44, 45]. All three isoforms of activated AKT (AKT1/2/3) have been associated with poor prognosis in neuroblastoma, but AKT2 regulates N-Myc expression in neuroblastoma cells and, therefore, is likely to be a key player in neuroblastoma biology [46]. Foley et al. demonstrated a link between micro-RNA 184 (miR-184), N-Myc, and AKT. N-Myc represses miR-184 and thereby increases levels of AKT2 (a direct target of miR-184 in neuroblastoma), increasing cell proliferation and survival [47]. Silencing AKT2 in neuroblastoma cells has been shown to impair cell proliferation, migration, and invasion [46]. In neuroblastoma, amplification of AKT commonly occurs, and activation of AKT correlates with poor patient outcome. Analysis of 116 primary neuroblastoma tissues demonstrated a high degree of phosphorylation of AKT in aggressive neuroblastoma, and a significant correlation was found between high levels of activated AKT and disease stage [44]. Chesler et al. reported that PI3K inhibition led to decreased tumor mass and reduced levels of N-Myc protein in a N-Myc murine neuroblastoma model [48]. Thus, the fact that SD exert their effect on neuroblastoma through their impact on AKT signaling is likely to have translational relevance.

We used a nano-delivery system to administer SD parenterally and demonstrated this led to a reduction of neuroblastoma tumor growth and inhibition of AKT activation *in vivo.* The drug was given twice daily at a dose of 5 mg/kg per dose, roughly equivalent to the low micromolar doses that led to a reduction of cytotoxicity and AKT activation in neuroblastoma cells grown in culture. Based on our findings, we conclude that SD may have efficacy in neuroblastoma.

Relatively little is known about the metabolism of SD. There is evidence that SD are incorporated into C18:2 ceramides in mammals and other species [49, 50] and that they preferentially accumulate in the mitochondria of BAX/BAK double knockout mouse epithelial cells [51]. These findings suggest the possibility that SD could influence the regulation of apoptosis, consistent with our previous reports [21, 22]. However, it has been reported that steady-state concentrations of SD-containing ceramides are only minor components of the plasma ceramide pool [52]. Long chain bases are normally catabolized through phosphorylation by sphingosine kinase and subsequent degradation by S1P lyase [53]. We are not aware of any reports demonstrating that SD-phosphate formation is the major route of its catabolism, but we speculate that this does occur and could therefore create unusual long chain base phosphates that could be biologically active and/or competitive with endogenous phosphorylated long chain bases in interacting with targets, receptors and/or enzymes. SD may also be excreted unchanged, i.e., without being metabolized to another species [54]. Further study will be required to assess the safety and efficacy of SD-NP in the treatment of neuroblastoma and other malignant diseases.

Supplementary Material

Refer to Web version on PubMed Central for supplementary material.

Acknowledgments

This study was supported by St. Baldricks Fellowship Grant 245216 (AEA), National Institutes of Health grants R01CA129438, S10OD018070 and Swim Across America Foundation (JDS) and National Institutes of Health grant R37 HL-64159 (ROR).

References

1. Matthay KK, George RE, Yu AL. Promising therapeutic targets in neuroblastoma. Clin Cancer Res. 2012; 18(10):2740–53. [PubMed: 22589483]
2. Ries LA, , et al. Cancer incidence and survival among children and adolescents: United States SEER Program 1975–1995. Bethesda, MD: National Cancer Institute; 1999. SEER Program, NIH Pub. No. 99 4649 192
3. Young JL Jr, Miller RW. Incidence of malignant tumors in U. S. children. Journal of Pediatrics. 1975; 86(2):254–8. [PubMed: 1111694]
4. Cheung NK, Dyer MA. Neuroblastoma: developmental biology, cancer genomics and immunotherapy. Nat Rev Cancer. 2013; 13(6):397–411. [PubMed: 23702928]
5. Frappaz D, et al. LMCE3 treatment strategy: results in 99 consecutively diagnosed stage 4 neuroblastomas in children older than 1 year at diagnosis. Journal of Clinical Oncology. 2000; 18(3):468–76. [PubMed: 10653862]
6. Speleman F, De Preter K, Vandesompele J. Neuroblastoma genetics and phenotype: a tale of heterogeneity. Semin Cancer Biol. 2011; 21(4):238–44. [PubMed: 21839839]
7. Maris JM, et al. Neuroblastoma. Lancet. 2007; 369(9579):2106–20. [PubMed: 17586306]

8. Maris JM. Recent advances in neuroblastoma. New England Journal of Medicine. 2010; 362(23): 2202–11. [PubMed: 20558371]
9. Stram DO, et al. Consolidation chemoradiotherapy and autologous bone marrow transplantation versus continued chemotherapy for metastatic neuroblastoma: a report of two concurrent Children's Cancer Group studies. Journal of Clinical Oncology. 1996; 14(9):2417–26. [PubMed: 8823319]
10. Zheng W, et al. Ceramides and other bioactive sphingolipid backbones in health and disease: lipidomic analysis, metabolism and roles in membrane structure, dynamics, signaling and autophagy. Biochim Biophys Acta. 2006; 1758:1864–1884. [PubMed: 17052686]
11. Durrant LG, Noble P, Spendlove I. Immunology in the clinic review series; focus on cancer: glycolipids as targets for tumour immunotherapy. Clin Exp Immunol. 2012; 167(2):206–15. [PubMed: 22235996]
12. Ogretmen B, Hannun YA. Biologically active sphingolipids in cancer pathogenesis and treatment. Nat Rev Cancer. 2004; 4(8):604–16. [PubMed: 15286740]
13. Symolon H, et al. Dietary soy sphingolipids suppress tumorigenesis and gene expression in 1,2-dimethylhydrazine-treated CF1 mice and ApcMin/+ mice. Journal of Nutrition. 2004; 134(5): 1157–61. [PubMed: 15113963]
14. Hakomori S. Glycosylation defining cancer malignancy: new wine in an old bottle. Proceedings of the National Academy of Sciences of the United States of America. 2002; 99(16):10231–3. [PubMed: 12149519]
15. Gilman AL, et al. Phase I study of ch14.18 with granulocyte-macrophage colony-stimulating factor and interleukin-2 in children with neuroblastoma after autologous bone marrow transplantation or stem-cell rescue: a report from the Children's Oncology Group. Journal of Clinical Oncology. 2009; 27(1):85–91. [PubMed: 19047298]
16. Yu AL, et al. Anti-GD2 antibody with GM-CSF, interleukin-2, and isotretinoin for neuroblastoma. N Engl J Med. 2010; 363(14):1324–34. [PubMed: 20879881]
17. Barker E, et al. Effect of a chimeric anti-ganglioside GD2 antibody on cell-mediated lysis of human neuroblastoma cells. Cancer Res. 1991; 51(1):144–9. [PubMed: 1988079]
18. Tettamanti G. Ganglioside/glycosphingolipid turnover: new concepts. Glycoconjugate Journal. 2004; 20(5):301–17. [PubMed: 15229395]
19. Chun J, et al. Synthesis of new trans double bond sphingolipid analogues: D4,6 and D6 ceramides. J Org Chem. 2002; 67:2600–2605. [PubMed: 11950306]
20. Struckhoff AP, et al. Novel ceramide analogs as potential chemotherapeutic agents in breast cancer. Journal of Pharmacology and Experimental Therapeutics. 2004; 309(2):523–32. [PubMed: 14742741]
21. Fyrst H, et al. Natural sphingadienes inhibit Akt-dependent signaling and prevent intestinal tumorigenesis. Cancer Research. 2009; 69(24):9457–64. [PubMed: 19934323]
22. Kumar A, et al. Chemopreventive sphingadienes downregulate Wnt signaling via a PP2A/Akt/GSK3beta pathway in colon cancer. Carcinogenesis. 2012; 33(9):1726–35. [PubMed: 22581840]
23. Vivanco I, Sawyers CL. The phosphatidylinositol 3-Kinase AKT pathway in human cancer. Nat Rev Cancer. 2002; 2(7):489–501. [PubMed: 12094235]
24. Bender A, et al. PI3K inhibitors prime neuroblastoma cells for chemotherapy by shifting the balance towards pro-apoptotic Bcl-2 proteins and enhanced mitochondrial apoptosis. Oncogene. 30(4):494–503. [PubMed: 20856197]
25. Nguyen TS, et al. Amphotericin B induces interdigitation of apolipoprotein stabilized nanodisk bilayers. Biochim Biophys Acta. 2008; 1778(1):303–12. [PubMed: 17980702]
26. Oskouian B, et al. Sphingosine-1-phosphate lyase potentiates apoptosis via p53- and p38-dependent pathways and is downregulated in colon cancer. Proc Natl Acad Sci U S A. 2006; 103:17384–17389. [PubMed: 17090686]
27. Jiang Q, et al. gamma-Tocopherol or combinations of vitamin E forms induce cell death in human prostate cancer cells by interrupting sphingolipid synthesis. Proc Natl Acad Sci U S A. 2004; 101(51):17825–30. [PubMed: 15596715]
28. Ryan RO, Forte TM, Oda MN. Optimized bacterial expression of human apolipoprotein A-I. Protein Expr Purif. 2003; 27(1):98–103. [PubMed: 12509990]

29. Lalefar NR, et al. Wnt3a nanodisks promote ex vivo expansion of hematopoietic stem and progenitor cells. J Nanobiotechnology. 2016; 14(1):66. [PubMed: 27553039]
30. Suh JH, et al. An LC/MS/MS method for quantitation of chemopreventive sphingadienes in food products and biological samples. J Chromatogr B Analyt Technol Biomed Life Sci. 2017; 1061–1062:292–299.
31. Soubeyran P, et al. Homeobox gene Cdx1 regulates Ras, Rho and PI3 kinase pathways leading to transformation and tumorigenesis of intestinal epithelial cells. Oncogene. 2001; 20(31):4180–7. [PubMed: 11464284]
32. Ryan RO. Nanobiotechnology applications of reconstituted high density lipoprotein. J Nanobiotechnology. 2010; 8:28. [PubMed: 21122135]
33. Ghosh M, Ryan RO. ApoE enhances nanodisk-mediated curcumin delivery to glioblastoma multiforme cells. Nanomedicine (Lond). 2014; 9(6):763–71. [PubMed: 23879635]
34. Singh AT, et al. Curcumin nanodisk-induced apoptosis in mantle cell lymphoma. Leuk Lymphoma. 2011; 52(8):1537–43. [PubMed: 21699455]
35. Oda MN, et al. Reconstituted high density lipoprotein enriched with the polyene antibiotic amphotericin B. J Lipid Res. 2006; 47(2):260–7. [PubMed: 16314670]
36. Li MH, Hla T, Ferrer F. Sphingolipid modulation of angiogenic factor expression in neuroblastoma. Cancer Prev Res (Phila). 2011; 4(8):1325–32. [PubMed: 21576349]
37. Villullas IR, et al. Characterisation of a sphingosine 1-phosphate-activated Ca2+ signalling pathway in human neuroblastoma cells. Journal of Neuroscience Research. 2003; 73(2):215–26. [PubMed: 12836164]
38. Rahmaniyan M, Qudeimat A, Kraveka JM. Bioactive Sphingolipids in Neuroblastoma. In: Shimada H, editorNeuroblastoma - Present and Future. InTech; Rijeka, Croatia: 2012. 153–184.
39. Li MH, Hla T, Ferrer F. FTY720 inhibits tumor growth and enhances the tumor-suppressive effect of topotecan in neuroblastoma by interfering with the sphingolipid signaling pathway. Pediatr Blood Cancer. 2013; 60(9):1418–23. [PubMed: 23704073]
40. Lee JH, et al. Effects of sphingosine-1-phosphate on neural differentiation and neurite outgrowth in neuroblastoma cells. Chonnam Med J. 2011; 47(1):27–30. [PubMed: 22111053]
41. Ponnusamy S, et al. Sphingolipids and cancer: ceramide and sphingosine-1-phosphate in the regulation of cell death and drug resistance. Future Oncol. 2010; 6(10):1603–24. [PubMed: 21062159]
42. Czubowicz K, Strosznajder R. Ceramide in the Molecular Mechanisms of Neuronal Cell Death. The Role of Sphingosine-1-Phosphate. Molecular Neurobiology. 2014:1–12.
43. Kraveka JM, et al. Involvement of dihydroceramide desaturase in cell cycle progression in human neuroblastoma cells. Journal of Biological Chemistry. 2007; 282(23):16718–28. [PubMed: 17283068]
44. Fransson S, et al. Aggressive neuroblastomas have high p110alpha but low p110delta and p55alpha/p50alpha protein levels compared to low stage neuroblastomas. J Mol Signal. 8(1):4. [PubMed: 23597230]
45. Opel D, et al. Activation of Akt predicts poor outcome in neuroblastoma. Cancer Research. 2007; 67(2):735–45. [PubMed: 17234785]
46. Qiao J, et al. Akt2 regulates metastatic potential in neuroblastoma. PLoS One. 2013; 8(2):e56382. [PubMed: 23468863]
47. Foley NH, et al. MicroRNA-184 inhibits neuroblastoma cell survival through targeting the serine/threonine kinase AKT2. Mol Cancer. 2010; 9:83. [PubMed: 20409325]
48. Chesler L, et al. Inhibition of phosphatidylinositol 3-kinase destabilizes Mycn protein and blocks malignant progression in neuroblastoma. Cancer Research. 2006; 66(16):8139–46. [PubMed: 16912192]
49. Sugawara T, et al. Intestinal absorption of dietary maize glucosylceramide in lymphatic duct cannulated rats. Journal of Lipid Research. 2010; 51(7):1761–9. [PubMed: 20211933]
50. Fyrst H, et al. Identification and characterization by electrospray mass spectrometry of endogenous Drosophila sphingadienes. J Lipid Res. 2008; 49(3):597–606. [PubMed: 18156591]

51. Zhang T, et al. Regulation of mitochondrial ceramide distribution by members of the BCL-2 family. J Lipid Res. 2015; 56(8):1501–10. [PubMed: 26059977]

52. Quehenberger O, et al. Lipidomics reveals a remarkable diversity of lipids in human plasma. J Lipid Res. 2010; 51(11):3299–305. [PubMed: 20671299]

53. Serra M, Saba JD. Sphingosine 1-phosphate lyase, a key regulator of sphingosine 1-phosphate signaling and function. Adv Enzyme Regul. 2010; 50(1):349–62. [PubMed: 19914275]

54. Sugawara T, et al. Digestion of maize sphingolipids in rats and uptake of sphingadienine by Caco-2 cells. Journal of Nutrition. 2003; 133(9):2777–82. [PubMed: 12949364]

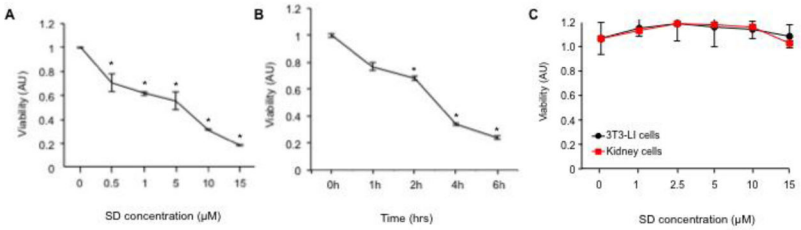

Figure 1. SD are cytotoxic to neuroblastoma cells but not non-malignant cells

(A) Dose response of SD-mediated cytotoxicity. Exponentially growing Kelly cells were exposed to a range of SD concentrations (0–15 μM). After 24 h incubation, cell viability was assessed by MTS assay. Results are presented as arbitrary units (AU). * P values: $p < 0.001$ for 0.5 μM; $p = 0.02$ for 1 μM; $p < 0.001$ for 5 μM; $p = 2 \times 10^{-6}$ for 10 μM; $p < 2 \times 10^{-6}$ for 15 μM. The results shown are representative of three similar experiments; n = 3 for each point. (B) Time-dependent inhibition of viability in response to SD treatment. Exponentially growing Kelly cells were treated with 10 μM SD or vehicle and incubated for 0–6 h, and viability was determined by MTS assay. * P values: $p < 0.02$ for 2h; $p = 1 \times 10^{-5}$ for 4h; $p = 3 \times 10^{-7}$ for 6h. The results shown are representative of three similar experiments; n = 3 for each point. (C) NIH 3T3 fibroblasts and primary human kidney cells established as described in Methods were exposed to a range of SD concentrations from 0–15 μM. After 24 h, cell viability was assessed by the MTS assay. The results shown are representative of three similar experiments; n = 3 for each point. There is no significant difference in SD-treated vs. vehicle-treated NIH3T3 or kidney cells at any concentration.

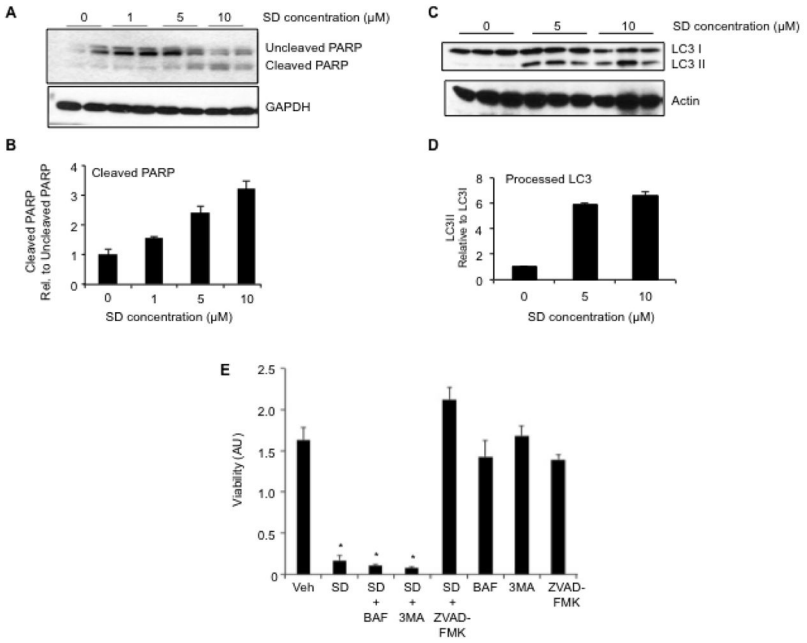

Figure 2. SD mediate cytotoxicity by inducing apoptosis in neuroblastoma cells

Kelly cells were grown to 70% confluence in DMEM plus 10% FCS, then changed to serum-free medium and treated with vehicle or varying concentrations of SD. Cells were harvested at 6 h, and whole cell extracts were analysed by immunoblotting to detect (A–B) uncleaved and cleaved PARP as an indicator of apoptosis, or (C–D) unprocessed and processed LC3 as an indicator of autophagy. Actin is used as a loading control. (B) and (D) represent image quantification of immunoblots shown in (A) and (C), respectively. In each case, the ratio of cleaved PARP to uncleaved PARP or LC3II to LC3I in the vehicle sample was arbitrarily set at one. These experiments were repeated at least three times with similar results. (E) Kelly neuroblastoma cells were pre-treated with either autophagy inhibitors bafilomycin (BAF, 1 μM) or 3-methyladenine (3MA, 1 mM), or with the pan-caspase inhibitor of apoptosis Z-VAD-FMK (100 μM) for 2 h, followed by treatment with either 10 μM SD or vehicle. Cells were incubated for an additional 12 h, harvested and evaluated for viability by MTS assay. This experiment was repeated at least three times with similar results.

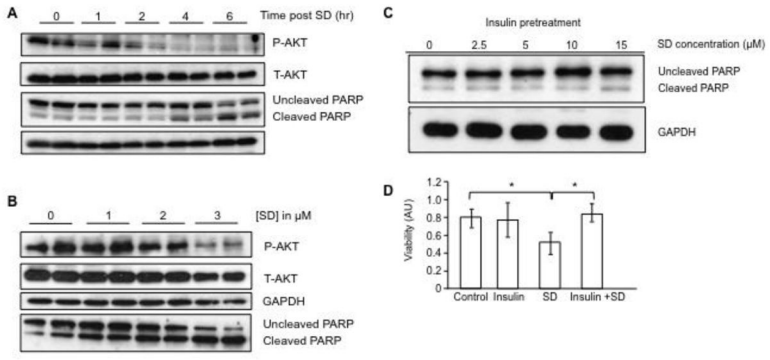

Figure 3. SD mediate cytotoxicity in neuroblastoma cells by inhibiting AKT signaling

(A) Kelly cells were grown to 70% confluence in the preferred medium plus 10% FCS, switched to serum-free medium, treated with 10 μM SD and incubated for an additional 0, 1, 2, 4 or 6 h. Cells were harvested at the designated time point, and whole cell extracts were analyzed by immunoblotting for total AKT (T-AKT) and phosphorylated AKT (P-AKT) and cleaved and uncleaved PARP. (B) Kelly cells were grown as described in (A) and after incubation in serum-free medium for 8 h were then treated with 0–3 μM SD for 20 h. Cells were harvested and whole cell extracts were analyzed by immunoblotting for T-AKT, P-AKT and cleaved and uncleaved PARP. (C) Kelly cells were serum starved for 12 h, pre-treated with insulin (2 μg/ml) for 1 h, followed by treatment with SD (0–15 μM). After 6 h of incubation, cells were harvested, and cleaved and uncleaved PARP were measured by immunoblotting of whole cell extracts. GAPDH was used as loading control. (D) Kelly cells received either no pre-treatment (control), insulin (2 μg/ml) pre-treatment for 1 h to activate AKT signaling, 10 μM SD without pre-treatment, or insulin pre-treatment followed by SD treatment. Cells were incubated for an additional 6 h, and cell viability was determined by the MTS assay. $*p < 0.05$. These experiments were repeated at least three times with similar results.

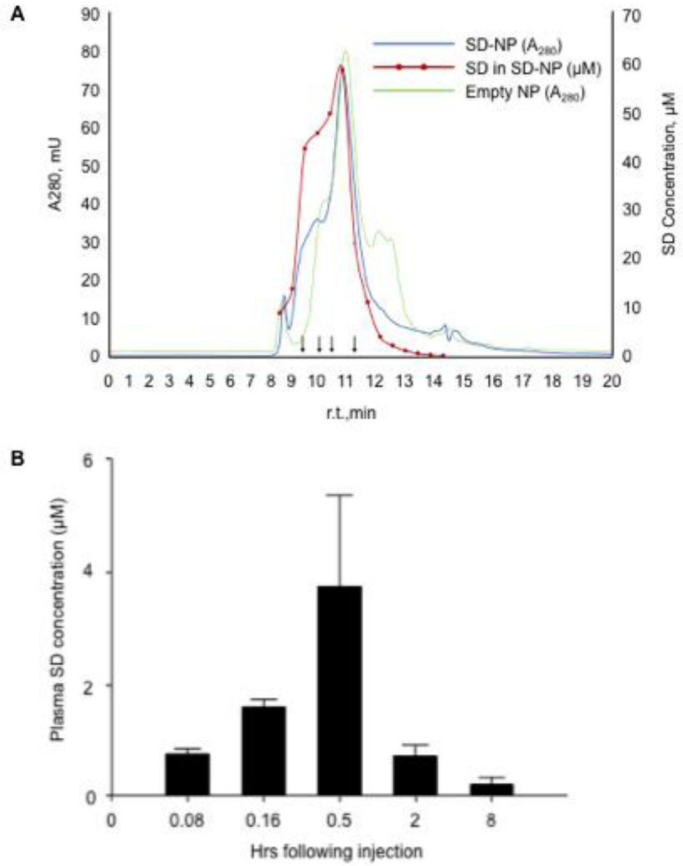

Figure 4. Characterization and kinetics SD-NP

(A) SD-NP were subjected to HPLC on a GF-250 size-exclusion column with continuous monitoring of protein absorbance at 280 nm (blue line). The red line is a plot of the SD content of specified fractions (filled red circles) determined by LC/MS/MS analysis. The SD concentration in μM is shown on the right hand Y axis. The chromatograph depicted in green corresponds to the 280 nm absorbance profile of control ND lacking SD while the black arrows depict the elution position of molecular weight standards (330, 199.5, 133 and 66.5 kDa). (B) Plasma SD levels determined by LC/MS after delivery to wild type mice by i.p. route as described in Methods.

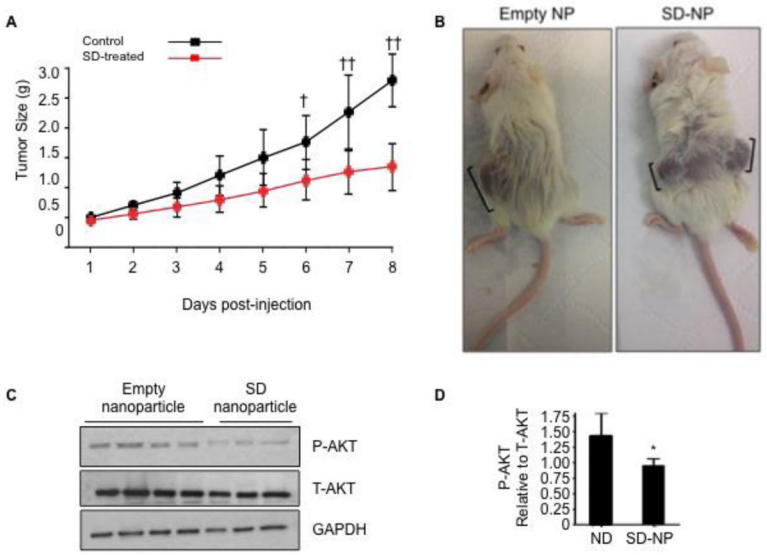

Figure 5. SD delivered via SD-NP inhibit tumor growth and AKT signaling in neuroblastoma xenografts *in vivo*

(A) Adult NOD/SCID mice were injected subcutaneously with 2 million Kelly cells suspended 1:1 (v/v) in matrigel. Xenograft tumor growth was assessed daily by calipers. Mice were randomly assigned to groups and received either SD-NP (10 mg/kg/d) or vehicle by i.p. injection twice daily starting when tumors were 100 mm^3 in size and continuing for approximately 8 d. Average tumor size in SD-NP treated mice (n = 17) are shown in red circles, and vehicle-treated mice (n = 3) are shown in black circles. Statistical analysis was performed using two-way ANOVA followed by Tukey's post-test. †, $p < 0.05$ for control vs. SD-NP; ††, $p < 0.0001$ for control vs. SD-NP. (B) Shown are representative tumors from one control mouse (in this case harboring a single xenograft in one flank) treated with empty NP and one SD-NP treated-mouse (harboring xenograft tumors in both flanks). Brackets show longest diameter of each tumor. (C) Adult NOD/SCID mice were implanted with Kelly xenografts as described in (A). When tumors were 100 mm^3 in size, mice either received a single dose of empty NP (n = 4) or SD-NP (n = 3) by i.p. injection. Mice were euthanized by CO_2 inhalation 8 h after administration of SD-NP or empty NP. Tumors were excised and flash frozen for molecular analysis. Whole tumor extracts were analyzed by immunoblotting to detect total AKT (T-AKT) or phosphorylated AKT (P-AKT). GAPDH was used as a loading control. (D) Image quantification of P-AKT/ T-AKT in immunoblot shown in (C).

Table 1

Hematology, blood chemistry and liver function tests in SD-treated and control mice.

Hematology										
	WBC (K/ul)	**Hb (g/dL)**	**Hematocrit %**	**Platelets (K/uL)**	**RBC (M/ul)**	**RDW %**	**MCV (fL)**	**MCH (pg)**	**MCHC (g/dL)**	**MPV (fL)**
Control	6.4±0.7	13.8±0.6	37.7±2.7	816± 273	10.0±0.7	17.9±0.2	37.6±0.3	13.7±0.9	36.5±2.2	6.6±0.2
Treatment	13.5±1.7*	14.3±0.6	38.5±2.8	809±197	10.6±0.7	19.4±0.8*	36.5±0.7	13.6±0.4	37.2±1.6	5.6±0.2*

	Neutrophil %	**Lymphocyte %**	**Monocyte %**	**Eosinophil %**	**Basophil %**
Control	13.2 ±2.2	74.907±6.9	9.3±1.9	1.9±2.0	0.8±1.2
Treatment	16.1 ±1.2		6.5±2.0	1.7±0.8	0.7±0.3

Blood Chemistry and Liver Functions											
	ALT U/L	**AST U/L**	**Albumin g/dL**	**Alkaline Phosphatase U/L**	**BUN mg/dL**	**Calcium mg/dL**	**Creatinine mg/dL**	**Glucose mg/dL**	**Phosphorus mg/dL**	**Total Bili mg/dL**	**Total Protein g/dL**
Control	30.1±13	151.5±9	3.8±0.1	103.8±19.7	20.9±2.0	11.7±0.5	0.1±0.4	305±46	10.1±1.1	0.1±0.1	6.0±0.2
Treatment	49.1±17	133.2±51	3.4±0.3	59.9±7.3*	35.1±7.0*	10.6±0.6	0.1±0.0	247±37	8.9±0.7	0.1±0.0	5.1±0.5*

†Mice received five doses of either empty ND (control) or SD-ND (treatment) as described in Methods. Blood was taken five days after the final dose and analyzed by the University of California at Davis Comparative Pathology Laboratory (CPL). All results for both control and treatment groups are within the normal limits for Balb/c mice as reported by the CPL.

*Significant differences between the two groups ($p < 0.05$) are designated with an asterisk. Control (n=3). Treatment (n=3).